DOI:
10.1063/1.4962864

Document Version
Publisher's PDF, also known as Version of record

AIP | Review of Scientific Instruments

A wide-field TCSPC FLIM system based on an MCP PMT with a delay-line anode

Wolfgang Becker, Liisa M. Hirvonen, James Milnes, Thomas Conneely, Ottmar Jagutzki, Holger Netz, Stefan Smietana, and Klaus Suhling

Citation: Review of Scientific Instruments **87**, 093710 (2016); doi: 10.1063/1.4962864
View online: http://dx.doi.org/10.1063/1.4962864
View Table of Contents: http://scitation.aip.org/content/aip/journal/rsi/87/9?ver=pdfcov
Published by the AIP Publishing

A wide-field TCSPC FLIM system based on an MCP PMT with a delay-line anode

Wolfgang Becker,[1] Liisa M. Hirvonen,[2] James Milnes,[3] Thomas Conneely,[3] Ottmar Jagutzki,[4] Holger Netz,[1] Stefan Smietana,[1] and Klaus Suhling[2]
[1]*Becker & Hickl GmbH, Nahmitzer Damm 30, 12277 Berlin, Germany*
[2]*Department of Physics, King's College London, Strand, London WC2R 2LS, United Kingdom*
[3]*Photek Ltd., 26 Castleham Rd., Saint Leonards-on-Sea TN38 9NS, United Kingdom*
[4]*Institut für Kernphysik, Max-von-Laue-Str. 1, 60438 Frankfurt, Germany*

(Received 10 May 2016; accepted 2 September 2016; published online 23 September 2016)

We report on the implementation of a wide-field time-correlated single photon counting (TCSPC) method for fluorescence lifetime imaging (FLIM). It is based on a 40 mm diameter crossed delay line anode detector, where the readout is performed by three standard TCSPC boards. Excitation is performed by a picosecond diode laser with 50 MHz repetition rate. The photon arrival timing is obtained directly from the microchannel plates, with an instrumental response of ~190 to 230 ps full width at half maximum depending on the position on the photocathode. The position of the photon event is obtained from the pulse propagation time along the two delay lines, one in x and one in y. One end of a delay line is fed into the "start" input of the corresponding TCSPC board, and the other end is delayed by 40 ns and fed into the "stop" input. The time between start and stop is directly converted into position, with a resolution of 200–250 μm. The data acquisition software builds up the distribution of the photons over their spatial coordinates, x and y, and their times after the excitation pulses, typically into 512 × 512 pixels and 1024 time channels per pixel. We apply the system to fluorescence lifetime imaging of cells labelled with Alexa 488 phalloidin in an epi-fluorescence microscope and discuss the application of our approach to other fluorescence microscopy methods. [http://dx.doi.org/10.1063/1.4962864]

I. INTRODUCTION

Imaging techniques based on fluorescence detection have found broad application in life sciences because they are extremely sensitive and are able to deliver information about biochemical interactions on the molecular scale. The techniques can further be refined by recording not only the fluorescence intensity or the fluorescence spectrum but also the fluorescence decay in the individual pixels of the image. The advantage of lifetime recording is that molecular parameters are directly represented by the parameters of the fluorescence decay functions[1–5] and that the results are independent of the fluorophore concentration which is difficult to control in cells and tissues.

There are a number of different techniques to detect the fluorescence lifetime and to combine fluorescence lifetime detection with imaging. Fluorescence Lifetime Imaging (FLIM) techniques can be divided into time-domain and frequency-domain techniques,[6–9] photon counting[10,11] and analog techniques,[6,12–15] and point-scanning[7,16] and wide-field imaging techniques.[6,12,15,17] It also matters whether a technique acquires the signal waveform in a few time gates[10] or in a large number of time channels[11,18] and whether this happens simultaneously[10,11,18] or sequentially.[12,15,17] Virtually all combinations are in use. This leads to a wide variety of instrumental principles.[2,19–21] Different principles differ in their photon efficiency, i.e., in the number of photons required for a given lifetime accuracy,[22–27] the acquisition time required to record these photons, the photon flux they can be used at, their time resolution, their ability to resolve the parameters of multi-exponential decay functions, multi-wavelength capability, optical sectioning capability, suppression of light scattered inside the sample, and compatibility with different imaging and microscopy techniques.[2,16,21]

The technique with the highest photon efficiency—important due to the limited photon budget emitted by the sample before it is irreversibly bleached[28]—and the highest time resolution is the combination of multi-dimensional time-correlated single photon counting (TCSPC) with confocal or multiphoton laser scanning.[11,16,18,26,29] Multi-dimensional TCSPC[11] is an extension of the classic (one-dimensional) TCSPC technique.[30] The sample is repetitively scanned by a high-repetition rate pulsed laser beam, single photons of the fluorescence signal are detected, and each photon is characterised by its time in the laser pulse period and the coordinates of the laser spot in the scanning area at the moment of its detection. The recording process builds up a photon distribution over these parameters. The photon distribution can be interpreted as an array of pixels, each containing a full fluorescence decay curve in a large number of time channels.

TCSPC-based FLIM with laser scanning suppresses out-of-focus signals and laterally scattered light,[16] resolves multi-exponential decay functions into their components, is able to record multi-wavelength FLIM data[11,29,31] and fast dynamic processes in a sample,[16,29,32,33] and can be used to record FLIM and PLIM (phosphorescence lifetime imaging)

images simultaneously.[29,34] Moreover, this technique is able to record FLIM at enormous pixel numbers and thus to obtain diffraction-limited resolution over the full field of view of a microscope lens.[16,35]

Despite this outstanding performance, there are FLIM applications where point scanning is not possible, cumbersome, or not desirable. Examples are single-molecule imaging or tracking experiments, light-sheet microscopy, prism-type total internal reflection fluorescence (TIRF) microscopy, recording of very slow phosphorescence phenomena, or recording of dynamic processes that occur at a time scale faster than the frame rate of a scanner. For these applications, it is desirable to have a combination of TCSPC with wide-field imaging available.

Recent developments use arrays of single-photon avalanche photodiodes (SPADs) with integrated time-to-digital converters (TDCs).[36] SPAD arrays can, in principle, achieve enormous global count rates well into the gigahertz region. Current SPAD arrays still have relatively low pixel numbers and can suffer from a low fill factor, noise, a large number of "hot" pixels, and non-uniformity of the pixel sensitivity. Although wide-field TCSPC FLIM with SPAD arrays has been demonstrated,[37] their main applications are currently in the military sector, in particular for range-finding and detection of hidden objects. Consumer electronics such as mobile phones also benefit from TCSPC-based range finding, where sensitivity is not as big an issue as it is with FLIM.[38]

Wide-field imaging based on photon counting with conventional photomultiplier tube (PMT)-based detectors has been around for more than a decade.[39] These techniques are based on single-photon detection by a photocathode, electron multiplication by a microchannel plate (MCP), and generation of a position signal for each photon. The data acquisition software builds up the distribution of the photon number over the image coordinates. The position information can be derived from images imprinted by the detection events in an intensified fast-readout camera,[24] from the electric charge of the individual photon pulses at the outputs of a quadrant anode,[40] a wedge-and-strip anode,[41] or a resistive anode of a MCP PMT.

To obtain FLIM data, in addition to the spatial position, the arrival time of the individual photons relative to the excitation pulses is determined. The arrival time is added as an additional coordinate of the photon distribution. The time resolution obtained by fast-readout cameras is on the order of 1 μs.[24] The time resolution can be increased to about 300 ns by exploiting the decay function of the phosphor in the intensifier output screen as an additional timing reference,[42] and lifetimes down to 450 ns have been measured with this approach.[43] This is not enough to record nanosecond fluorescence decay data of the commonly used fluorescence markers and of endogenous fluorophores in biological specimens. Only the position-sensitive MCP-PMT is fast enough to record fluorescence decay curves at picosecond resolution.

Position-readout via a quadrant anode, a wedge-and-strip anode, a cross strip anode, or a resistive anode requires charge detection by low-noise charge-sensitive amplifiers, analog-to-digital conversion, and calculation of ratios of the signals. These are time-consuming operations. The maximum count rate of such systems is therefore low.[44] Another way to obtain position information is to couple the single-photon pulses into two crossed delay lines at the detector output. The position is determined by measuring the relative arrival times of the photon pulses at the four outputs of the delay lines.[41,44,45] The delay lines can be placed inside the detector or outside the detector and coupled capacitively to a resistive anode inside the detector.[41,45] The delay-line technique requires relatively complex recording electronics but works up to a count rate of more than 1 MHz, and commercially available standard TCSPC boards can be employed to perform this task.

In this paper, we describe a FLIM system based on an MCP detector with position readout via delay lines and recording of the position and timing signals by TCSPC. The instrument integrates all the components needed to perform FLIM experiments in bio-medical applications. It contains the excitation light source, the optics, the detector, the TCSPC system, and the software for data acquisition, system control, and data analysis.

II. SYSTEM ARCHITECTURE

A. MCP PMT with position readout via delay-lines

The instrument described here is based on the FGN 392-1000 detector from Photek, UK. The FGN 392-1000 is a 40 mm diameter MCP PMT with position readout via two crossed delay lines. The principle of the detector is shown in Fig. 1(a).

Photoelectrons leaving the photocathode are accelerated towards a microchannel plate by a high voltage. The MCP consists of an array of narrow channels (12 μm diameter) with a conductive coating on the inside. A high voltage is applied across the MCP. The electrical field forces the photoelectrons into the channels. As the electrons move through the channels, they bounce between the channel walls and get multiplied by secondary electron emission. Two microchannel plates are connected in series so that a total gain on the order of 10^6 is achieved at total voltage of 3000 V.

When the electron cloud leaves the low-side of the second MCP, it generates an electrical pulse at the timing output. This pulse is used to determine the arrival time of the photon, typically with a resolution of a few tens of picoseconds.[11] Moreover, the electron cloud is accelerated towards a resistive anode. The distance between the photocathode and first MCP is around 0.1 mm, minimising the photoelectron trajectory spread, while the distance between the last MCP and the resistive anode is around 4 mm, allowing the charge cloud to spread out.[45] The anode is capacitively coupled to a system of two crossed delay lines outside the tube. Note that the delay lines do not have to be bakeable or vacuum-compatible and can be embedded in a printed circuit board. The charge cloud is thus transferred into the delay lines to create pulses which propagate along the delay line. The arrival times at the delay line outputs indicate the spatial position where the electron cloud hits the anode. While a delay line can be a helical wire, here we use a printed circuit anode with LC elements connecting the strips at 2 mm distance, as illustrated in Fig. 1(b). The charge cloud footprint typically has a diameter of a few mm, i.e., larger

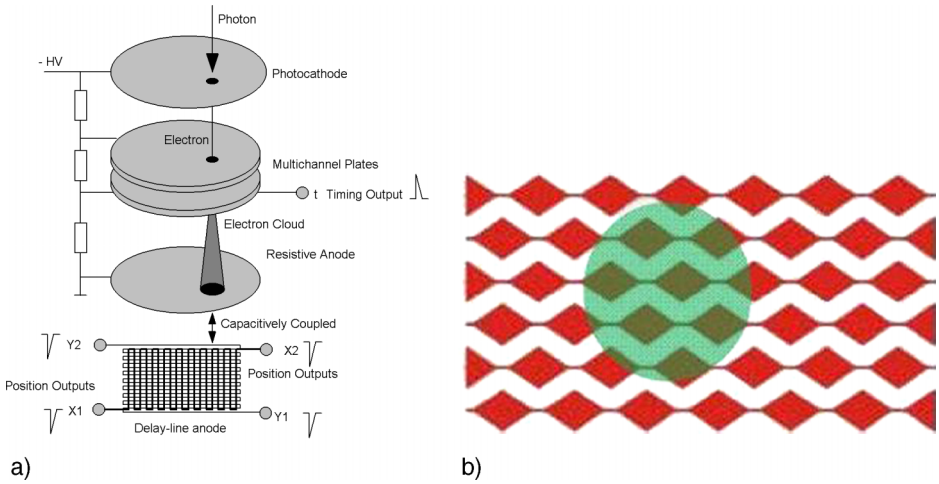

FIG. 1. (a) Principle of the position-sensitive MCP-based detector. The detector has a delay-line structure as an anode. The X position of a photon is proportional to the delay between X1 and X2. The Y position of a photon is proportional to the delay between Y1 and Y2. The time of the photon is derived from a signal from the low-side of the microchannel plate, t. (b) A schematic of the delay line. The diamonds represent LC elements, and the green circle is the footprint of the electron cloud, adapted from Ref. 45.

than the delay line wire pitch.[46] If the charge cloud is spread out over several discrete pick-up structures, it is possible to achieve a position resolution which is not limited by the pitch or width of the delay line—only by the time resolution of the electronics, provided there is sufficient gain from the MCP.[44]

B. TCSPC system

The architecture of the TCSPC system is shown in Fig. 2. The system consists of three SPC-150N modules[29] from Becker & Hickl, Germany. The first module measures the arrival times, t, of the photons in the laser pulse period. The second and third modules measure the relative propagation times, t_x and t_y, of the pulses at the outputs of the X and the Y delay lines. Delay cables in the stop input of the TCSPC board, with the same transit time as the delay lines, guarantee that the start-stop times remain positive for all X and Y positions. The data from the three TCSPC modules are transferred into the system computer photon by photon. Every photon is characterised by a "micro time" which is the start-stop time at the picosecond time scale within the laser pulse period, a "macro time" which is the absolute time from the start of the experiment, and additional bits which identify photons recorded by different detectors or excited by different multiplexed lasers.[29] The micro times of the first module represent t, the micro times of the second and third modules represent x and y. The data acquisition software receives these data triples and builds up a photon distribution over the coordinates, x, y, and the times, t. This is the usual photon distribution of the well known and characterised scanning TCSPC-based FLIM. It is an array of pixels each of which contains a fluorescence decay curve consisting of photon numbers in consecutive time channels.

C. Matching of detection events in the TCSPC channels

For correct build-up of the photon distribution, it is important that the software matches the detected events from the three TCSPC modules correctly and assigns the t, x, and y values from the individual SPC modules correctly to the individual photons. Moreover, there may be detected events with pulse amplitudes close to the thresholds of the constant fraction discriminators (CFDs). It can happen that such events do not trigger all CFDs of all TCSPC modules so that the t, x, y information remains incomplete.

Matching of the events is achieved by using the macro times of the events in the individual TCSPC modules. The signal transit time over the full length of the detector delay lines is about 40 ns, the external delay in the stop lines of the

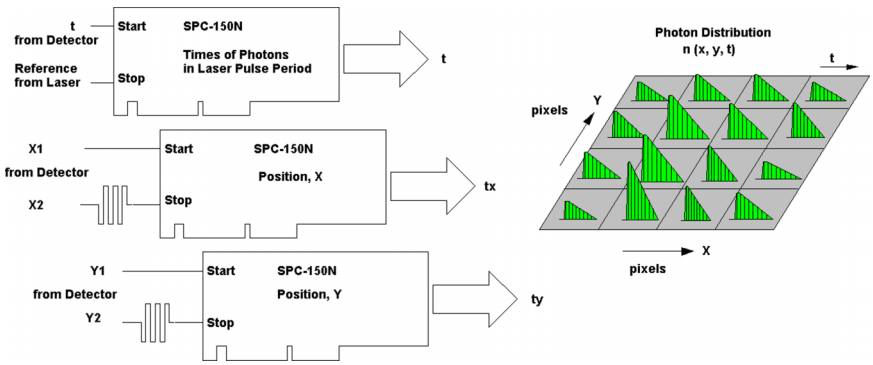

FIG. 2. Schematic of the operating principle of the wide-field TCSPC system.

x and y channels is also 40 ns. Therefore the stop in the x and y modules occurs 40–80 ns after a photon was detected. For a laser pulse period of 20 ns, this is 20 ns–80 ns after the stop in the t channel. The following procedure is used to match the events:

(1) Identify a photon in the t channel, note the macro time, T_t.
(2) Look for events in the x and y channels that have macro times, T_x and T_y, in the range from $T_t + 20$ to $T_t + 80$ ns.
(3) If x and y events in this macro time interval are found, the data triple, t, x, y, is used to address the memory location in the photon distribution to which the photon is added.
(4) If no x or no y event is found in the interval, the data of this photon are discarded.

To make this process work, the measurement in all three modules must be started at exactly the same moment, and the macro-time clocks in the modules must be synchronised. This is achieved by using the "Trigger Master" and "Clock Master" functions of the SPC-150N modules.[29,47]

D. Constant-fraction discriminators

The single-photon pulses of PMTs have a substantial amplitude jitter. Moreover, there is a large fraction of low-amplitude pulses that originate from thermal emission of the photocathode. All TCSPC modules therefore use CFDs at their start and stop inputs. The CFDs not only reject noise and low-amplitude pulses but also prevent the amplitude jitter of the detector pulses from inducing timing jitter. The principle of a CFD is shown in Fig. 3.

The CFD has two discriminators, D1 and D2, and two delay lines, Delay1 and Delay2. D1 selects pulses, the amplitude of which exceeds a selectable "CFD threshold." Moreover, the input pulses travel through the delay lines. The second discriminator, D2, measures the difference of the signals at the input and output of Delay2. The difference has a bipolar shape with a zero transition, the temporal position of which is independent of the pulse amplitude. The output of D2 triggers a D flip-flop if D1 has responded. The CFD thus delivers an output pulse when the difference voltage crosses the "CFD zero cross" level and the input amplitude has exceeded the "CFD threshold." This implementation is equivalent to the conventional principle where the input pulse is split into two components, one being attenuated and the other being inverted and delayed. These two pulses are then added together, with the zero crossing point providing the constant fraction trigger. For correct CFD function, the delay of Delay2 has to be on the order of the leading-edge time of the detector pulses. For the timing output of the Photek FGN 392-1000 detector, this is about 2 ns, as shown in Fig. 4. The delay lines are made of meander lines on the printed circuit boards of the discriminators. In the Becker & Hickl SPC-150N modules, the entire CFD is a 4 cm × 4 cm module that is plugged on the printed circuit board of the TCSPC module.

The CFD principle shown in Fig. 3 requires that the input pulses are reasonably clean, with a reasonably steep leading edge, and negligible ringing. This is the case for the pulses at the timing output of the detector (Fig. 4) but, unfortunately, not for the signals at the outputs of the delay lines. The signal shape at the X1 output is shown in Fig. 5(a). The signal resembles a burst of pulses rather than a typical single photon pulse. The reason for the strange signal shape is that the electron cloud of a single photoelectron simultaneously hits several parts of the delay line structure, see Fig. 1(b). Moreover, the subsequent steps of the delay line are electrically not perfectly de-coupled, which introduces further ringing in the signal. Trying to process a signal like this by the CFD principle shown in Fig. 3 is hopeless because there is no unambiguous zero transition at the input of the zero cross discriminator.

The only way to obtain timing from the position outputs is to determine the centroid of the entire burst. This can be achieved by sending the signal through a low-pass filter (pulse shape shown in Fig. 5(b)) and processing the resulting pulse by a CFD, the delay lines of which are adapted to the slow rise time of the filtered signal. An approach like this has been used in Ref. 44. The disadvantage is that the delay lines of the CFD become inconveniently long. The rise time of the filtered signal is on the order of 10 ns, corresponding to an electrical path length of about 2 m. Therefore the CFDs cannot be squeezed into the size of the printed circuit boards of the SPC-150N discriminators.

To make the CFDs of the X and Y channels compatible with the SPC-150N TCSPC boards, we used LC-filter structures instead of cables or meander lines. These are small enough to fit into the available size of the CFDs and act as filters and delay lines simultaneously. The SPC-150N boards can thus be modified to work with the position signals of the FGN 392-1000 detector by simply replacing the CFDs. The principle of the X and Y CFDs is shown in Fig. 6.

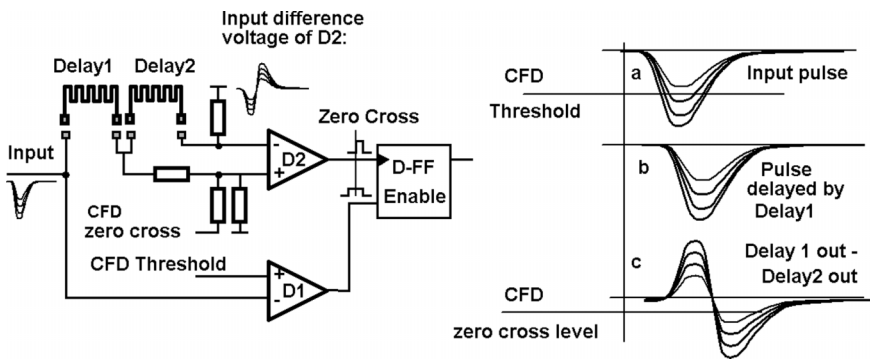

FIG. 3. Principle of a constant-fraction discriminator (CFD).

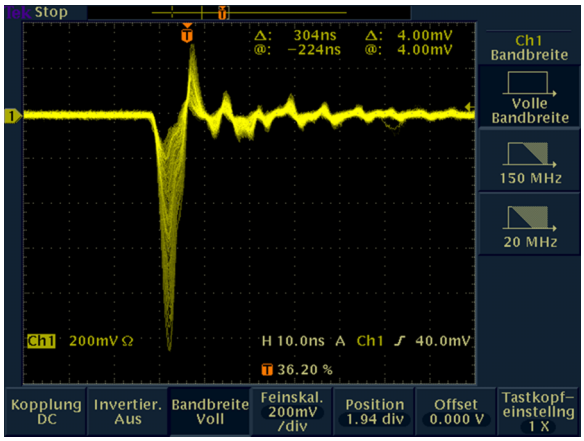

FIG. 4. Single-photon pulse shape at the timing output of the Photek FGN 392-1000 detector. The leading-edge time is approximately 2 ns. Note the amplitude jitter of the pulses. Recorded with a Tektronix TDS 3052 oscilloscope, bandwidth 500 MHz.

Filter 1 converts the input burst into a continuous waveform. The pulse shape at the output of Filter 1 is smooth enough to trigger the threshold discriminator, D1. The pulses are further filtered and simultaneously delayed by Filter/Delay1 and Filter/Delay2. The difference voltage at the inputs of the zero cross discriminator is clean enough to provide unambiguous zero cross triggering.

E. Optical system

The optical part of the wide-field FLIM system is shown in Fig. 7. It consists of a Nikon TE 2000 inverted microscope, a Becker & Hickl BDS-SM 488 nm picosecond diode laser, and the Photek FGN 392-1000 detector. The BDS-SM laser provides the excitation light. It delivers light pulses of 50 MHz repetition rate and approximately 60 ps optical pulse width. A filter in the excitation path removes long-wavelength wideband background from the laser beam. The light passing the filter is delivered into the microscope by a single-mode fibre. The microscope beam-splitter cube reflects the laser towards the microscope objective. The fibre output delivers a diverging beam of light into the back aperture of the microscope objective such that it illuminates the entire field of view. Due to the clean beam profile at the end of the single-mode fibre, the illumination is sufficiently uniform over the entire image area.

Fluorescence excited in the sample is collected by the objective and passes through the dichroic mirror of the beam-splitter cube and an emission filter. It is directed out of the microscope via one of its side ports. An achromatic concave lens of a few cm focal length in front of the image plane magnifies the image to match the active area of the detector. A shutter is placed behind the lens to conveniently block the detection light path when the microscope lamp is used. For the images presented in this work, we used a Nikon CFI Plan Fluor $20\times$ NA = 0.5 microscope lens.

Unlike a confocal scanning system, a wide-field system has no pinhole that suppresses light scattered in the optics. It is therefore important to insert baffles in the optical path to block spurious signals that bounce off the edges of lenses or the walls of optical tubes.

F. Implementation in the TCSPC data acquisition software

Becker & Hickl SPCM TCSPC data acquisition software was used to run the system. SPCM controls the three SPC-150N TCSPC cards, builds up the photon distribution, and displays the data online. Moreover, it allows us to control the laser power, adjust the detector operating voltage, and to operate the shutter from the software user interface. SPCM uses 64-bit Windows technology and thus can easily accommodate the large size of FLIM data.[29,35]

Wide-field FLIM was implemented as an "Operation Mode" in the Becker & Hickl SPCM TCSPC data acquisition software. The definition of the imaging and timing parameters is similar to the procedure used for the first in, first out (FIFO) imaging modes used in combination with optical scanners.[29] Image formats up to 2048×2048 pixels can be defined. The available number of time channels is 256 for 2048×2048 pixels and increases to 1024 channels and 4096 channels for images sizes of 1024×1024 pixels and 512×512 pixels, respectively. As for the other operation modes, system parameters special to the selected operation mode are defined under "More Parameters." For the wide-field FLIM

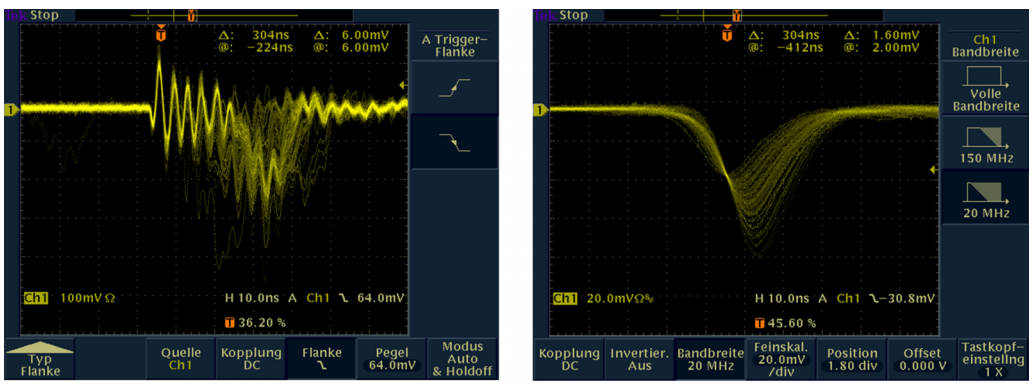

a) b)

FIG. 5. (a) Single photon pulses at the X1 output of the FGN 392-1000 detector. (b) Signal after passing through a 20 MHz low-pass filter. Recorded with a Tektronix TDS 3052 oscilloscope, bandwidth 500 MHz.

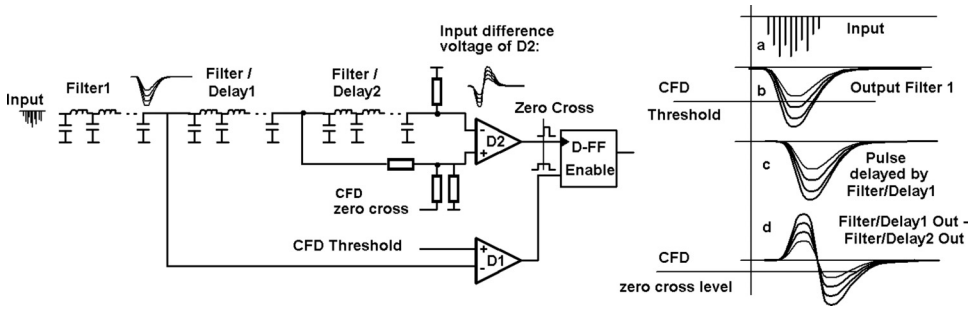

FIG. 6. CFD of X and Y channels. The input signal is low-pass filtered by Filter 1 and delayed and further filtered by Filter/Delay1 and Filter/Delay2. The timing pulse is derived from the difference voltage Filter/Delay1 Out minus Filter/Delay2 Out.

mode, the "More Parameters" field defines which of the three TCSPC modules is the timing channel, the X channel, and the Y channel. It also defines the timing range for the X- and Y-channel modules. A "matching interval" defines the macro time interval for the parameter-tag data of the modules that are considered to belong to one and the same photon.

During the measurement, the data acquisition software reads the photon data from the three TCSPC modules, assigns the data to the individual photons by their macro times, and builds up the photon distribution. Images are displayed in selectable time intervals, typically one to 3 s. The build-up of the images can thus directly be observed by the operator. The data acquisition can be stopped by an operator command or after a pre-defined collection time. It is also possible to repeat the entire process automatically and save the data in a sequence of files. For preview purposes, images can be acquired and displayed in intervals of 1 s or less. This fast preview function is essential—without a fast preview function it is not possible to achieve accurate focusing, sample positioning, and excitation power adjustment within a sufficiently short period of time.

III. RESULTS

A. Temporal instrument response function

The temporal instrument response function (IRF) of the detection system was recorded by pointing the attenuated laser beam (1 mm diameter, pulse width 60 ps) to different locations on the photocathode. To avoid saturation of the microchannel plates by a high local intensity, the IRF measurement was performed at a count rate of no more than 70 kHz. A typical result is shown in Fig. 8.

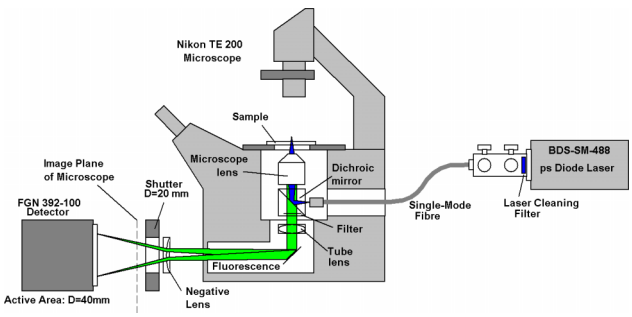

FIG. 7. Optical system consisting of a pulsed excitation source, an inverted microscope, and the crossed delay line detector.

The full-width at half-maximum (FWHM) is 187–233 ps. These values contain a small contribution from the convolution with the optical laser pulse which is, however, no larger than 10 ps. The IRF curves show that there is a noticeable change in the IRF shape and position with the X position on the photocathode. The shift in the first moment of the IRF is about 75 ps.

B. Cell imaging

Fig. 9 shows FLIM data of BPAE (bovine pulmonary artery epithelium) cells labelled with Alexa 488 phalloidin (F36924, Invitrogen), recorded by the wide-field TCSPC system. Data analysis was performed by Becker & Hickl SPCImage software, which is an integrated part of the SPCM TCSPC package.[29] An intensity image built-up from the TCSPC data is shown left, and a lifetime image is shown right. A decay curve for the pixel at the cursor position is shown at the bottom. The decay curve is clean, without optical or electrical reflections. The residuals of a double exponential fit (shown below the decay curve) confirm the good quality of the temporal data. However, some smears possibly from out-of-focus fluorescence or spurious reflection inside the optical system can be seen in the image. This is not unexpected—a wide-field epi-fluorescence system is much more vulnerable to these effects than a confocal or multiphoton scanning system.

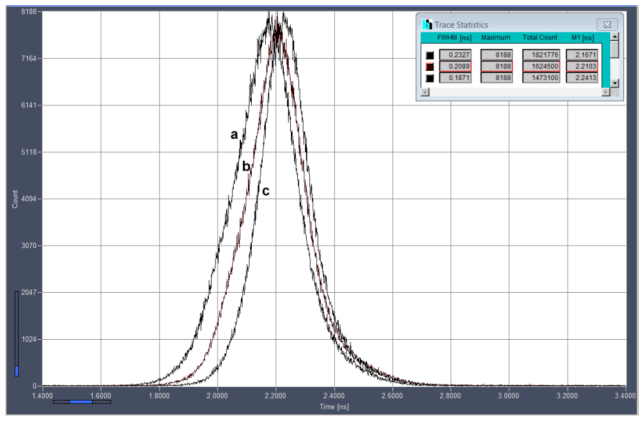

FIG. 8. Temporal instrument response function (IRF) for different X positions on the photocathode. a, b, c: x = 0, 0.5, 1 of field diameter, respectively. Y position y = 0.5. Full width at half maximum (FWHM) is 233 ps (a), 209 ps (b), and 187 ps (c).

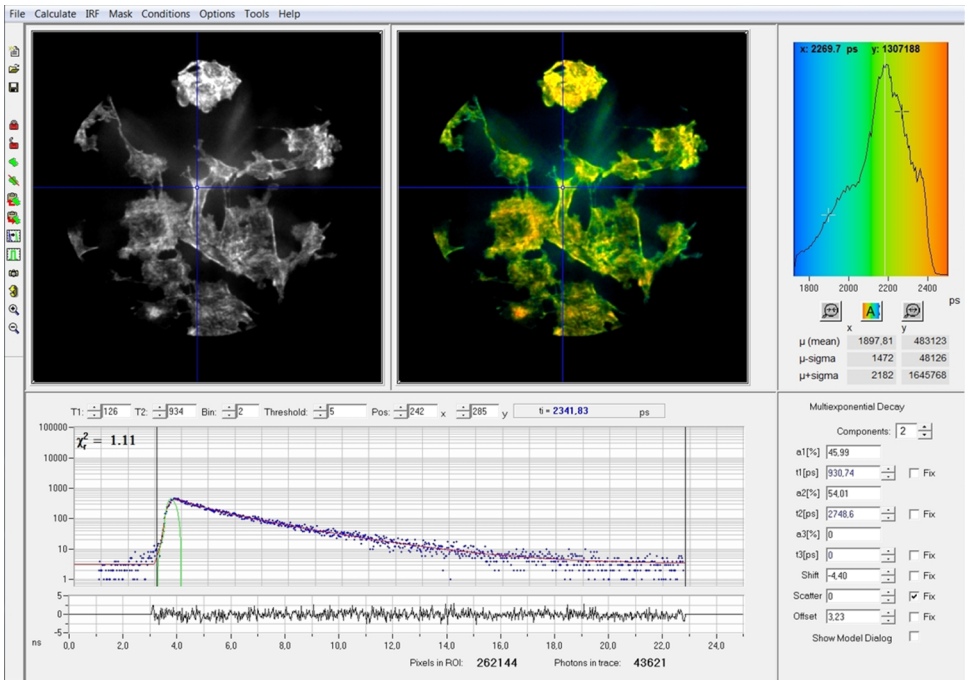

FIG. 9. BPAE sample labelled with Alexa 488 phalloidin (Invitrogen F36924), data analysis by SPCImage. 512×512 pixels, 1024 time channels per pixel. Analysis with double-exponential decay model, floating IRF.

C. Spatial resolution

The fluorescence lifetime image is shown at larger scale in Fig. 10. The image was recorded at a TCSPC resolution of 512 × 512 pixels and 1024 time channels per pixel. The active area of the detector covers about 440 × 440 pixels. A 5× digital zoom into a region near the centre of the image is shown in Fig. 11. The smallest details seen in the zoom image appear about three pixels (full width at half maximum) wide. The intrinsic resolution of the detector/TCSPC combination can be estimated to be 270 μm on the active area of the detector. This is 1/150 of the diameter of the active detector area. A TCSPC resolution of 512 × 512 pixels is thus sufficient to obtain Nyquist-sampled image data. Spatial oversampling with a TCSPC resolution of 1024 × 1024 or 2048 × 2048 pixels is, in principle, possible but does not further improve the spatial resolution.

IV. DISCUSSION

Delay line anode detectors obtain the photon position from the signal propagation time along the delay line, i.e., the spatial localisation is accomplished by arrival timing of electronic pulses. We show here that it is feasible to carry out

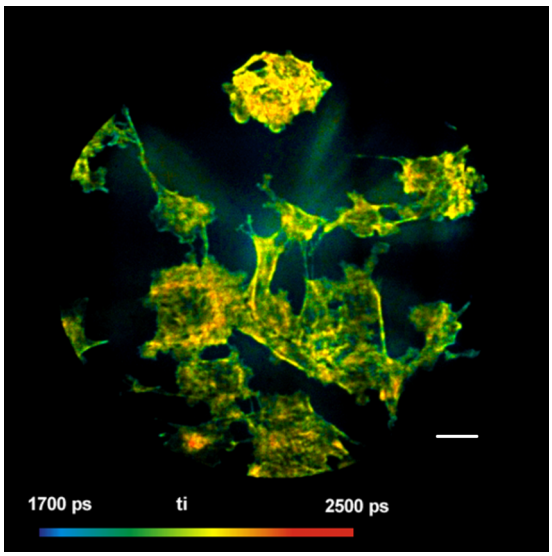

FIG. 10. Wide-field FLIM image obtained with a 20× NA = 0.5 objective and analysed with the parameters shown in Fig. 9. 512×512 pixels, intensity-weighted fluorescence lifetime of double-exponential decay. Diameter of the field of view is 200 μm, and scale bar is 20 μm.

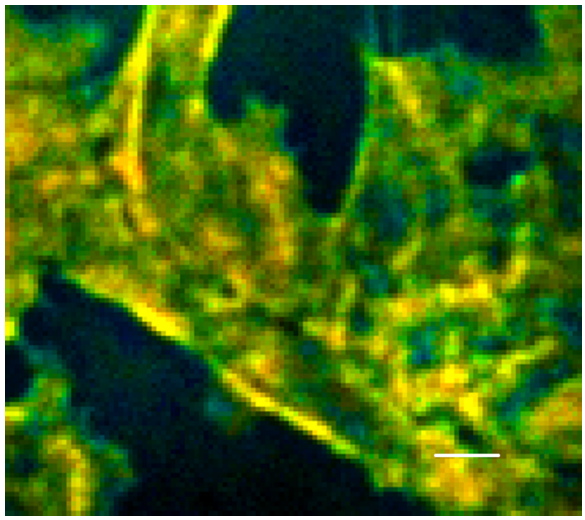

FIG. 11. 5× zoom into an image area near the centre of Fig. 10. The smallest details appear around 3 pixels wide, indicating a spatial resolution of the detector/TCSPC combination in the range of about 1/150 of the entire image area. Scale bar 4 μm.

the arrival timing with conventional TCSPC boards, by simply connecting the delay line output, with a suitable delay and appropriately designed and optimised pulse shaping and timing CFD electronics, to the TCSPC timing board. Converting the localisation problem to a timing problem eliminates the need for dedicated charge amplitude measurement electronics, as in position sensitive detectors employing charge division approaches.[39]

The spatial and the temporal resolution of the wide-field TCSPC system are lower than for TCSPC scanning systems. First, the spatial resolution of wide-field microscopy is lower than for confocal microscopy, in general. Second, scanning systems obtain spatial and temporal resolution by separate elements. These can be optimised independently, resulting in exquisitely optimised spatial and temporal resolution. Wide-field TCSPC obtains spatial and temporal resolutions in one and the same detector, which necessarily requires some trade-off between spatial readout performance and time resolution. On one hand, a relatively large detector area is needed to obtain good spatial resolution for a given minimum size of the delay line structures; on the other hand, a large size results in location-dependent propagation-time and an increase in pulse rise time for the timing output. We believe that these parameters can be improved by further optimising the CFDs and by using preamplifiers with lower noise.

It should be noted here that the recording process described above works only if the probability to detect two photons in the same laser pulse period is negligible. If this is not the case, photons in the later part of the fluorescence decay are lost, and the recorded waveform gets distorted. This "pile up" effect has been subject of discussion for many years.[11,30] It has, however, been shown that the size of the effect is much smaller than commonly believed. Photon rates as high as 10% of the laser pulse frequency can be processed with no more than 2.5% error in the recorded fluorescence lifetime.[11,29]

Moreover, in case two photons occur in the same time window after an excitation pulse, the propagation time difference in each position channel will effectively yield one averaged position for the two photons. The chance that this happens is reduced by the dead time of the TCSPC modules (100 ns) and the event matching procedure. A photon detected within 100 ns after a previous one is not recorded. Photons falling into the dead time of one TCSPC channel but not into the dead time of another one are suppressed by the event matching procedure. We do not see signs of mismatched detection events up to a rate of 1 MHz averaged over the entire image area. A different timing board configuration would allow a total propagation time check, which would eliminate multiple photon detection and thus act as a pile up inspector.[48] The maximum count rate which can be reached with pile up inspectors is 37% of the laser repetition rate.[49]

The IRFs depend on the position of the photocathode. The shift in the first moment of the IRF is about 75 ps. There are two reasons for this shift. The first one is that the timing signal is derived from one side of the microchannel plate. Therefore there is a non-zero propagation delay from the detection position to the output signal line. The second one is that there is a systematic variation in the shape of the electrical single-photon pulse with the detection position. The shape variation causes a shift of the zero-cross point in the CFD. Due to both effects, the IRF is a function of the spatial position at which the photons are detected. A shift in the first moment of the IRF induces a shift of approximately the same size in the calculated fluorescence lifetimes. For the results presented here, we therefore used a floating IRF in the FLIM data analysis.[29] The resulting loss in lifetime accuracy is negligible for lifetimes longer than 1 ns but increases rapidly for lifetimes in the range of the IRF width and shorter. The location-dependent shift of the IRF can be removed by applying a position-dependent correction to the photon times in the acquisition process. A corresponding procedure is already used by the SPCM software to compensate propagation-time differences in multi-anode PMTs.[29] It can, in principle, also be used for wide-field FLIM.

As in all wide-field imaging systems, the excitation intensity is spread over the entire field of view, rather than being focused into a spot, as in scanning systems. However, the wide-field system suffers from the general problems of wide-field imaging:[16,29] Missing suppression of out-of-focus fluorescence and lateral scattering, and contamination by fluorescence and scattering in the optics.[16] These problems are not a feature of wide-field TCSPC, they are a problem of wide-field imaging in general. They can in principle be solved by structured-illumination techniques[50] and by image reconstruction techniques. However, these techniques involve the calculation of differences between images taken with different illumination patterns or between images taken in different focal planes. Applying such calculations to data that are dominated by photon noise results in a massive degradation of the signal-to-noise ratio and, consequently, of the photon efficiency. Other optical sectioning techniques such as temporal focussing, speckle illumination, Nipkow spinning disks, or multibeam scanning approaches may be better for achieving optically sectioned wide-field FLIM.

The conclusion is that wide-field FLIM should be used in applications where scanning is not applicable and which works with thin samples or samples with low scattering. Possible applications are prism-type TIRF microscopy and light-sheet microscopy which are inherently wide-field techniques. Prism-type TIRF can be performed with the system with minor modifications in the optical system, light sheet microscopy needs special beam shaping, and, typically, the acquisition of images of several focal planes. Objective-based TIRF and supercritical angle fluorescence would also be feasible with this approach.[51] The data acquisition does not pose major problems for the SPCM software. Either triggered sequential recording with the "autosave" function or "spatial mosaic" imaging can be used.[29]

Another application may be combined FLIM/PLIM with phosphorescence markers or up-converting nanoparticles of milli- or microsecond lifetimes.[34] Recording such data by scanning requires extremely low scan rates and long acquisition times but does not pose problems to wide-field FLIM. Wide-field FLIM may also be useful to record fast physiological processes in cells, for example, for recording chlorophyll transients in plants or transient changes in free Ca^{2+} in cells.[32]

In contrast to scanning, in a wide-field system, the time resolution for the phosphorescence decay or for a

physiological effect is not coupled to the pixel, line, or frame rate of a scanner. The timing information for the phosphorescence decay or for the physiological effect is available from the macro times of the photons and can be used to build-up a photon distribution with an additional time axis.

Wide-field TCSPC FLIM may also be useful for single-molecule spectroscopy or single molecule localisation experiments. In addition to the FLIM data, the SPCM software is able to store the parameter-tag single-photon data.[29] These contain information on the diffusion of the molecules, on conformational changes, intersystem crossing, and blinking.[25] Moreover, the exact position of the molecules can be determined at super-resolution precision by locating and centroiding the images of the individual molecules. Single-molecule localisation is facilitated by the large oversampling factors available in the SPCM software. The pixel number can be increased up to 1024 × 1024 or 2048 × 2048 pixels with 1024 and 256 time channels, respectively.

An extension of the system is possible by using several lasers which are multiplexed at a period in the microsecond range. Recording in the TCSPC modules is synchronised with the laser multiplexing via the routing inputs of the TCSPC modules. The data acquisition uses the routing information to store the photons of different lasers in separate photon distributions. The function could be used to simultaneously record FLIM images excited by different laser wavelengths or images excited under different polarisation.[29]

V. SUMMARY

The setup described is a fully functional wide-field TCSPC FLIM system, based on a crossed delay line anode detector readout with conventional TCSPC timing boards. This approach retains all the advantages of TCSPC and extends them to wide-field detection, serving essentially as a single photon sensitive camera with picosecond resolution. The operation of the system is fully integrated in the TCSPC acquisition software and allows rapid preview of the acquired images, an essential feature to facilitate focussing, sample positioning, and excitation power adjustment. Data are saved as a conventional x, y, t FLIM data cube, and data analysis is performed in the usual way by FLIM analysis software. The data obtained with the system feature good time resolution with an IRF below 230 ps and reasonably good spatial resolution below 270 μm over the 40 mm diameter detector. In common with other wide-field epi-fluorescence microscopy approaches, the excitation intensity is spread over the whole field of view, there is no suppression of out-of-focus fluorescence or lateral scattering, and there is contamination by fluorescence and scattering in the optics. The system is thus best used with thin samples with low internal scattering, e.g., for applications such as prism-type TIRF and light-sheet microscopy, combined FLIM/PLIM with phosphorescence markers or up converting nanoparticles of millisecond lifetimes, and the measurement of fast physiological processes in cells. Wide-field FLIM may also be applicable to single-molecule spectroscopy and singe-molecule localisation experiments.

ACKNOWLEDGMENTS

K.S. and L.M.H. acknowledge BBSRC Sparking Impact and EPSRC Impact Acceleration funding for this work.

[1]P. I. H. Bastiaens and A. Squire, Trends in Cell Biol. **9**, 48–52 (1999).
[2]W. Becker, J. Microsc. **247**(2), 119–136 (2012).
[3]M. Y. Berezin and S. Achilefu, Chem. Rev. **110**(5), 2641–2684 (2010).
[4]J. R. Lakowicz, *Principles of Fluorescence Spectroscopy*, 3rd ed. (Springer, New York, 2006).
[5]K. Suhling, L. M. Hirvonen, J. A. Levitt, P.-H. Chung, C. Tregido, A. Le Marois, D. A. Rusakov, K. Zheng, S. Ameer-Beg, S. Poland, and S. Coelho, in *Advanced Time-Correlated Single Photon Counting Applications*, edited by W. Becker (Springer International Publishing, Berlin, Heidelberg, New York, 2015), pp. 119–188.
[6]J. R. Lakowicz and K. Berndt, Rev. Sci. Instrum. **62**, 1727–1734 (1991).
[7]T. B. Krasieva, C. Stringari, F. Liu, C. H. Sun, Y. Kong, M. Balu, F. L. Meyskens, E. Gratton, and B. J. Tromberg, J. Biomed. Opt. **18**, 031107 (2013).
[8]E. Gratton and B. Barbieri, Spectroscopy **1**, 28–36 (1986).
[9]H. T. Chen, G. Holst, and E. Gratton, Microsc. Res. Tech. **78**(12), 1075–1081 (2015).
[10]E. P. Buurman, R. Sanders, A. Draaijer, H. C. Gerritsen, J. J. F. van Ween, P. M. Houpt, and Y. K. Levine, Scanning **14**, 155–159 (1992).
[11]W. Becker, *Advanced Time-Correlated Single Photon Counting Techniques* (Springer, Berlin, Heidelberg, New York, 2005).
[12]K. Dowling, S. C. W. Hyde, J. C. Dainty, P. M. W. French, and J. D. Hares, Opt. Commun. **135**(1-3), 27–31 (1997).
[13]Y. Sun, R. Liu, D. S. Elson, C. W. Hollars, J. A. Jo, J. Park, Y. Sun, and L. Marcu, Opt. Lett. **33**(6), 630–632 (2008).
[14]D. R. Yankelevich, D. S. Elson, and L. Marcu, in *Fluorescence Lifetime Spectroscopy and Imaging*, edited by L. Marcu, P. W. M. French, and D. S. Elson (CRC Press, Boca Raton, London, New York, 2015).
[15]A. D. Scully, A. J. Mac Robert, S. Botchway, P. O'Neill, A. W. Parker, R. B. Ostler, and D. Phillips, J. Fluoresc. **6**(2), 119–125 (1996).
[16]W. Becker, V. I. Shcheslavskiy, and H. Studier, in *Advanced Time-correlated Single Photon Counting Applications*, edited by W. Becker (Springer, Berlin, Heidelberg, New York, 2015).
[17]M. Straub and S. W. Hell, Appl. Phys. Lett. **73**(13), 1769–1771 (1998).
[18]W. Becker, A. Bergmann, M. A. Hink, K. König, K. Benndorf, and C. Biskup, Microsc. Res. Tech. **63**(1), 58–66 (2004).
[19]K. Suhling, P. M. W. French, and D. Phillips, Photochem. Photobiol. Sci. **4**, 13–22 (2005).
[20]L. Marcu, P. M. W. French, and D. S. Elson, *Fluorescence Lifetime Spectroscopy and Imaging: Principles and Applications in Biomedical Diagnostics* (CRC Press, Boca Raton, 2014).
[21]W. Becker and A. Bergmann, in *Handbook of Biomedical Nonlinear Optical Microscopy*, edited by B. R. Masters and P. T. C. So (Oxford University Press, Oxford, 2008).
[22]R. M. Ballew and J. N. Demas, Anal. Chem. **61**(1), 30–33 (1989).
[23]H. C. Gerritsen, N. A. H. Asselbergs, A. V. Agronskaia, and W. G. J. H. M. Van Sark, J. Microsc. **206**(3), 218–224 (2002).
[24]L. M. Hirvonen, F. Festy, and K. Suhling, Opt. Lett. **39**(19), 5602–5605 (2014).
[25]M. Prummer, C. G. Hübner, B. Sick, B. Hecht, A. Renn, and U. P. Wild, Anal. Chem. **72**(3), 443–447 (2000).
[26]E. Gratton, S. Breusegem, J. Sutin, Q. Ruan, and N. Barry, J. Biomed. Opt. **8**(3), 381–390 (2003).
[27]M. Köllner and J. Wolfrum, Chem. Phys. Lett. **200**(1-2), 199–204 (1992).
[28]Q. L. Zhao, I. T. Young, and J. G. S. de Jong, J. Biomed. Opt. **16**(8), 086007 (2011).
[29]W. Becker, *The bh TCSPC Handbook*, 6th ed. (Becker & Hickl GmbH, 2015).
[30]D. V. O'Connor and D. Phillips, *Time-Correlated Single-Photon Counting* (Academic Press, London, 1984).
[31]W. Becker, A. Bergmann, and C. Biskup, Microsc. Res. Tech. **70**(5), 403–409 (2007).
[32]W. Becker, V. Shcheslavskiy, S. Frere, and I. Slutsky, Microsc. Res. Tech. **77**(3), 216–224 (2014).
[33]S. Frere and I. Slutsky, in *Advanced Time-Correlated Single Photon Counting Applications*, edited by W. Becker (Springer, Berlin, Heidelberg, New York, 2015).
[34]V. I. Shcheslavskiy, A. Neubauer, R. Bukowiecki, F. Dinter, and W. Becker, Appl. Phys. Lett. **108**(9), 091111 (2016).

[35]H. Studier and W. Becker, Proc. SPIE **8948**, 89481K (2014).
[36]E. Charbon, M. Fishburn, R. Walker, R. Henderson, and C. Niclass, in *TOF Range-Imaging Cameras*, edited by F. Remondino and D. Stoppa (Springer, Berlin, Heidelberg, 2013), pp. 11–38.
[37]G. Giraud, H. Schulze, D. U. Li, T. T. Bachmann, J. Crain, D. Tyndall, J. Richardson, R. Walker, D. Stoppa, E. Charbon, R. Henderson, and J. Arlt, Biomed. Opt. Express **1**(5), 1302–1308 (2010).
[38]See http://www.st.com/content/st_com/en/about/media-center/press-item.html/stmicroelectronics-proximity-sensor-solves-smartphone-hang-ups.html for information about proximity sensing in mobile phones using photon time-of-flight measurements with SPAD arrays.
[39]X. Michalet, R. A. Colyer, G. Scalia, A. Ingargiola, R. Lin, J. E. Millaud, S. Weiss, O. H. W. Siegmund, A. S. Tremsin, J. V. Vallerga, A. Cheng, M. Levi, D. Aharoni, K. Arisaka, F. Villa, F. Guerrieri, F. Panzeri, I. Rech, A. Gulinatti, F. Zappa, M. Ghioni, and S. Cova, Philos. Trans. R. Soc., B **368**(1611), 20120035 (2013).
[40]V. Emiliani, D. Sanvitto, M. Tramier, T. Piolot, Z. Petrášek, K. Kemnitz, C. Duneux, and M. Coppey-Moisan, Appl. Phys. Lett. **83**(12), 2471–2473 (2003).
[41]J. Milnes, J. S. Lapington, O. Jagutzki, and J. Howorth, Nucl. Instrum. Methods Phys. Res., Sect. A **604**(1-2), 218–220 (2009).
[42]L. M. Hirvonen, Z. Petrášek, A. Beeby, and K. Suhling, New J. Phys. **17**(2), 023032 (2015).
[43]L. M. Hirvonen, Z. Petrášek, A. Beeby, and K. Suhling, Proc. SPIE **9329**, 932939 (2015).
[44]O. Jagutzki, V. Mergel, K. Ullmann-Pfleger, L. Spielberger, U. Meyer, R. Dörner, and H. Schmidt-Böcking, Proc. SPIE **3438**, 322–333 (1998).
[45]O. Jagutzki, A. Czasch, and S. Schössler, Proc. SPIE **8727**, 87270T (2013).
[46]S. Schössler, B. Bromberger, M. Brandis, L. P. H. Schmidt, K. Tittelmeier, A. Czasch, V. Dangendorf, and O. Jagutzki, J. Instrum. **7**, C02048 (2012).
[47]S. Felekyan, R. Kühnemuth, V. Kudryavtsev, C. Sandhagen, W. Becker, and C. A. M. Seidel, Rev. Sci. Instrum. **76**(8), 083104 (2005).
[48]B. van Meurs and R. van der Werf, J. Phys. E: Sci. Instrum. **9**(6), 437–438 (1976).
[49]C. C. Davis and T. A. King, J. Phys. A: Gen. Phys. **3**(1), 101–109 (1970).
[50]M. J. Cole, J. Siegel, S. E. D. Webb, R. Jones, K. Dowling, M. J. Dayel, D. Parsons-Karavassilis, P. M. W. French, M. J. Lever, L. O. D. Sucharov, M. A. A. Neil, R. Juškaitis, and T. Wilson, J. Microsc. **203**, 246–257 (2001).
[51]L. M. Hirvonen, W. Becker, J. Milnes, T. Conneely, S. Smietana, A. Le Marois, O. Jagutzki, and K. Suhling, Appl. Phys. Lett. **109**, 071101 (2016).